https://doi.org/10.26599/FRICT.2026.9441310
Research Article

Achieving macroscopic superlubricity on the steel surfaces with a functionally designed Ce-based emulsion

Jinjin Li [a], Rui Zhang [a], Wen Zhong [b], Yun Chen [b], Yongqiang Xin [c], Yongfeng Yang [a,b]*

[a]State Key Laboratory of Tribology in Advanced Equipment, Tsinghua University, Beijing 100084, China

[b]School of Mechanical Engineering, Xihua University, Chengdu 610039, China

[c]Chengdu High-Speed Train Depot of China Railway Chengdu Bureau Group Co., Ltd., 610057, China

Corresponding author E-mail: yfywind@xhu.edu.cn

Received: April 20, 2026; Revised: August 9, 2026; Accepted: September 2, 2026

Abstract: This study explored the achievement of macroscopic liquid superlubricity using a Ce-based emulsion at the steel/steel interface. The Ce-based emulsion was prepared with Poly-L-lysine (PLL), oleic acid (OA), and a cerium-based emulsifier. After an initial running-in period of approximately 300 s, a superlubricity state characterized by a minimum coefficient of friction (COF) of 0.001 and a maximum contact pressure up to 197 MPa was achieved. The superlubricity originated from the

synergistic adsorption of OA, PLL, and the emulsifier, driven by the C=C/COOH groups in OA, the amino-rich chains of PLL, and the Ce^{3+} containing head of the emulsifier. This cooperative adsorption promoted the formation of a hierarchical tribofilm that effectively separated the sliding surfaces under boundary lubrication. The study demonstrated the potential of emulsion-based lubricants for achieving ultra-low friction and wear in mechanical engineering applications.

Keywords: superlubricity; emulsion; cerium-based; Poly-L-lysine; oleic acid

1 Introduction

Friction and wear lead to considerable energy dissipation and economic costs, thereby enhancing the tribological properties of materials as a vital research focus with significant economic, societal, and environmental implications[1-3]. Superlubricity, characterized by a coefficient of friction below 0.01, is associated with negligible material wear[4-6]. Therefore, achieving superlubricity is essential for extending the operational lifespan of components and enhancing energy utilization efficiency[7, 8].

Liquid superlubricity is primarily achieved through the use of water-based or oil-based lubricants. Water-based lubricants mainly included phosphoric acid solution[9], glycerol solution, [10-12] polyalcohol solution, [13, 14] ionic liquid solution[15-17] and so on. The achievement of water-based superlubricity primarily relied on the hydration effect of the lubricant, where a tribochemical reaction occurred during the running-in phase to form a tribofilm at the friction interface. In addition, adding two-dimensional materials to water-based liquids as lubricant additives was a common way to achieve superlubricity. Examples of these materials included graphene[18], graphene oxide[19], boron nitride[20], black phosphorus[21].

Compared to water-based lubricants, the oil-based lubricants were more viscous and difficult to shear, so their contact pressures to achieve superlubricity were typically

lower. The main base oils used to realize oil-based superlubricity included oleic acid, vegetable oil, 1, 3-diketone oil, and poly alpha olefin (PAO)[22-28]. Li et al.[29] achieved macroscopic superlubricity on steel surfaces with engineering level roughness using 1, 3-diketone oil as a lubricant. Zeng et al.[30] achieved superlubricity using castor oil during the sliding of Ni-Ti alloys with steel. Long et al.[31] also obtained superlubricity using castor oil and attributed the superlubricity mechanism to the activation of the chemical degradation of castor oil by high localized pressure, which produced graphite/graphene-like material at the friction interface. Gao et al.[32] added oxidized black phosphorus to oleic acid and achieved superlubricity with a COF of 0.006 in 52100 steel/steel contact. Yi et al.[33] used alkyl-functionalized black phosphorus nanosheets as lubricating additives for PAO and achieved superlubricity on steel doped with diamond-like carbon film.

The above studies achieved superlubricity using both water-based and oil-based lubricants, where water-based lubricants exhibited low shear strength and cooling properties, while oil-based lubricants had good lubrication performance, with relatively poor fluidity and cooling performance. However, in machining equipment, both cooling and lubrication properties were highly demanded at the same time. In this regard, emulsions consisting of an aqueous phase, an oil phase, and an emulsifier were the good choice, which could provide both lubrication and cooling due to the unique properties of oil and water coexistence. Recently, Chen et al. [34] achieved a milestone by demonstrating macroscale superlubricity using a dual-responsive microemulsion, which opened a new avenue for smart lubricants. Microemulsions featured droplet sizes below 100 nm and were optically transparent, and their formation required precise ratios of oil, water, and surfactants. In contrast, conventional emulsions were opaque with larger droplet sizes (typically >100 nm), and were vastly more common in industrial applications such as metalworking fluids and food processing.

However, conventional emulsions had never been reported to achieve macroscopic liquid superlubricity. In this study, an emulsifier consisting of the rare earth element Ce

was synthesized and the emulsion was prepared by using a mixture of Poly-L-lysine, water and ethylene glycol as the aqueous phase and oleic acid as the oil phase. The emulsion successfully achieved macroscopic liquid superlubricity at the steel/steel interface after a running-in period of about 300 s, accompanied by the lowest COF of 0.001 and a maximum contact pressure of 197 MPa. In addition, the worn surface after emulsion lubrication was analyzed in detail to investigate the mechanism for achieving superlubricity. The contribution of each component (oil phase, PLL, and emulsifier) to the superlubricity performance was systematically evaluated.

2 Experimental

2.1 Materials

The Poly-L-lysine (average Mw~4500) and octadecene were purchased from Beijing Kaiguo Science and Technology Co., Ltd, China. The didodecyldimethylammonium chloride ($C_{26}H_{56}Cl{\cdot}N$), cerium chloride ($CeCl_3$), oleic acid (OA), stearic acid, ethylene glycol, methanol, and Sudan IV were purchased from Shanghai Aladdin's Reagent Co., Ltd, China. The octadecane and octadecene were provided from Beijing Bailing Wei Science and Technology Co., Ltd, China.

2.2 Preparation of emulsion

Before preparing the emulsion, the emulsifier didodecyl dimethyl cerium tetrachloride (DDCe, $(C_{12}H_{25})_2N^+(CH_3)_2$-$[CeCl_4]^-$) was first synthesized. Equimolar masses of didodecyldimethylammonium chloride and $CeCl_3$ were mixed in methanol and magnetically stirred at room temperature for 12 hours. Subsequently, the mixed liquid was dried in a desiccator under vacuum at 80 ºC for 12 hours to obtain a white solid powder, which was the emulsifier DDCe [34].

Then, the preparation of the aqueous phase (W-PLL) was carried out by mixing 10 wt% Poly-L-Lysine, 40 wt% water, 50 wt% ethylene glycol and ultrasonically mixing for 30 minutes. Next, to this aqueous phase, oil and DDCe (with equal mass fractions) were added at concentrations of 0.5 wt%, 1.0 wt%, 2.0 wt%, and 3.0 wt% to formulate

the emulsions. The oil phase consisted of four 18-carbon chain compounds: octadecane ($C_{18}H_{38}$), octadecene ($C_{18}H_{36}$, $CH_2=CH(CH_2)_{15}CH_3$, with a double bond), octadecanoic acid (stearic acid, $C_{18}H_{36}O_2$, $C_{17}H_{35}COOH$, with a carboxyl group), and octadecenoic acid (oleic acid, $C_{18}H_{34}O_2$, $CH_3(CH_2)_7CH=CH(CH_2)_7COOH$, with a double bond and a carboxyl group). These components were carefully selected for their chemical diversity. Finally, the mixture of oil phase, DDCe and W-PLL was stirred by ultrasonication for 30 minutes to obtain the emulsions. All the prepared emulsions remained homogeneous without observable phase separation for at least one month at room temperature, demonstrating excellent long-term stability.

2.3 Tribological tests

The tribological tests were conducted using a universal micro-tribometer (UMT-5, Bruker, USA) with a rotating mode. The AISI 52100 steel balls with a diameter of 6 mm and AISI 52100 steel disks with diameter of 24 mm were used as the friction pair. Before the friction tests, 30 μL of lubricant was added by micropipette to the contact area. The friction tests were conducted with a radius of 3 mm and a sliding speed that varied from 0.025 to 0.30 m/s. The applied normal loads ranged from 1–4 N (the maximum initial Hertzian contact pressure was about 1.04 GPa at 4 N, calculated by the Eq. (S1) Supporting Information). The test was repeated three times for each lubrication condition to ensure data validity.

2.4 Characterization

The prepared emulsions were tested for dynamic viscosity using an MCR-302 rheometer at room temperature (25 ℃). The surface functional groups of emulsions were tested by Fourier transform infrared spectroscopy (FTIR, X70). In order to observe the type of emulsification and the size of oil droplets in the emulsion, Sudan IV and ethanol were mixed and added to the emulsion to stain the oil phase, and then the stained droplets were dropped onto a slide and covered with a coverslip, and then

the distribution of oil phase and the size of the oil droplets in the emulsion were subsequently observed by using a VHX-9000 KEYENE microscope.

For the worn steel surfaces, the surface morphology and roughness were analyzed using a 3D white light interferometer (Nexview, ZYGO Lamda). The worn surfaces were also characterized by XPS to investigate the chemical compositions. In addition, a focused ion beam (FIB) -SEM dual system (LYRA3, TESCAN. Q.S., Czech Republic) was used to prepare the extracted lamellar cross-sectional specimens of the wear scar regions on the steel surfaces. The cross-sectional images of the prepared FIB specimens were obtained by high-resolution transmission electron microscopy (HRTEM).

3 Results and discussion

3.1 Characterization of the emulsions

The oil phase in the emulsions (EM) was stained red using Sudan IV, and the distribution of the oil phase with 18 carbon atoms in the aqueous phase could be clearly seen, as shown in Fig. 1 (a-h). It could be determined that all four prepared emulsions were oil-in-water type (O/W). Compared with EM-octadecene (octadecene emulsion) and EM-OA (oleic acid emulsion), fewer oil phases were distributed in EM-octadecane (octadecane emulsion) and EM-stearic acid (stearic acid emulsion), which indicated that the stability and homogeneity of these two emulsions were not good. The oil droplets in EM-octadecane were round, but the droplet sizes were not uniform, and the maximum particle size was 38.5 μm. EM-stearic acid did not form round oil droplets and the distribution was not uniform, indicating that stearic acid did not form a uniform and stable emulsion. EM-Octadecene formed uniform but large oil droplets with a maximum particle size of 26.0 μm. EM-OA formed uniform and small oil droplets with a maximum particle size of only 9.4 μm. In addition, the emulsions formed by different concentrations of OA were also observed microscopically, as shown in Fig. S1. With the increase of OA content, the oil droplet content in the aqueous phase increased gradually, and the maximum oil droplet size also increased gradually. At 3.0 wt% OA

concentration, the maximum oil droplet particle size reached 22.5 μm, and the distribution ratio of oil droplets in the figure was also high, almost filling the whole page. The dynamic viscosities of the EM-OA emulsions at different oil concentrations were measured, as shown in Fig. S2. The viscosity remained nearly unchanged at 16.8 mPa·s for 0.5 wt% and 1.0 wt%, and increased only slightly to 17.6 mPa·s at 2.0 wt% and 18.2 mPa·s at 3.0 wt%.

The dynamic viscosity (Fig. 1i) and FTIR spectra (Fig. 1j) of the four emulsions were tested. Because octadecane and stearic acid were solids at room temperature, the dynamic viscosity of the oil phase was tested only for octadecene and OA, where octadecene exhibited a lower viscosity (3.9 mPa·s) and OA exhibited a higher viscosity (32.8 mPa·s). The dynamic viscosity of the aqueous phase (W-PLL) was 14.0 mPa·s, and the dynamic viscosities of the four emulsions were similar and all were slightly higher than that of the aqueous phase. Among the emulsions, EM-stearic acid exhibited the highest viscosity at 18.6 mPa·s, while EM-Octadecene showed the lowest viscosity at 15.9 mPa·s. In the FTIR absorption spectrum, the broad absorption peak at 3400 cm^{-1} corresponded to the hydroxyl (-OH) stretching vibration, the characteristic peaks at 1090 cm^{-1} and 1040 cm^{-1} corresponded to the stretching vibration of the C-N/C-O bond, which were the characteristic peaks of the aqueous phase. The characteristic peak at 1700 cm^{-1} corresponded to the stretching vibration of the carbon-oxygen double bond (carboxyl group, -COOH), and 1640 cm^{-1} corresponded to the stretching vibration of the carbon-carbon double bond (C=C), which were the characteristic peaks of the oil phase. Therefore, there were both the characteristic peaks of the aqueous phase (-OH and C-N/C-O) and the oil phase (C=C and C=O) in the emulsions.

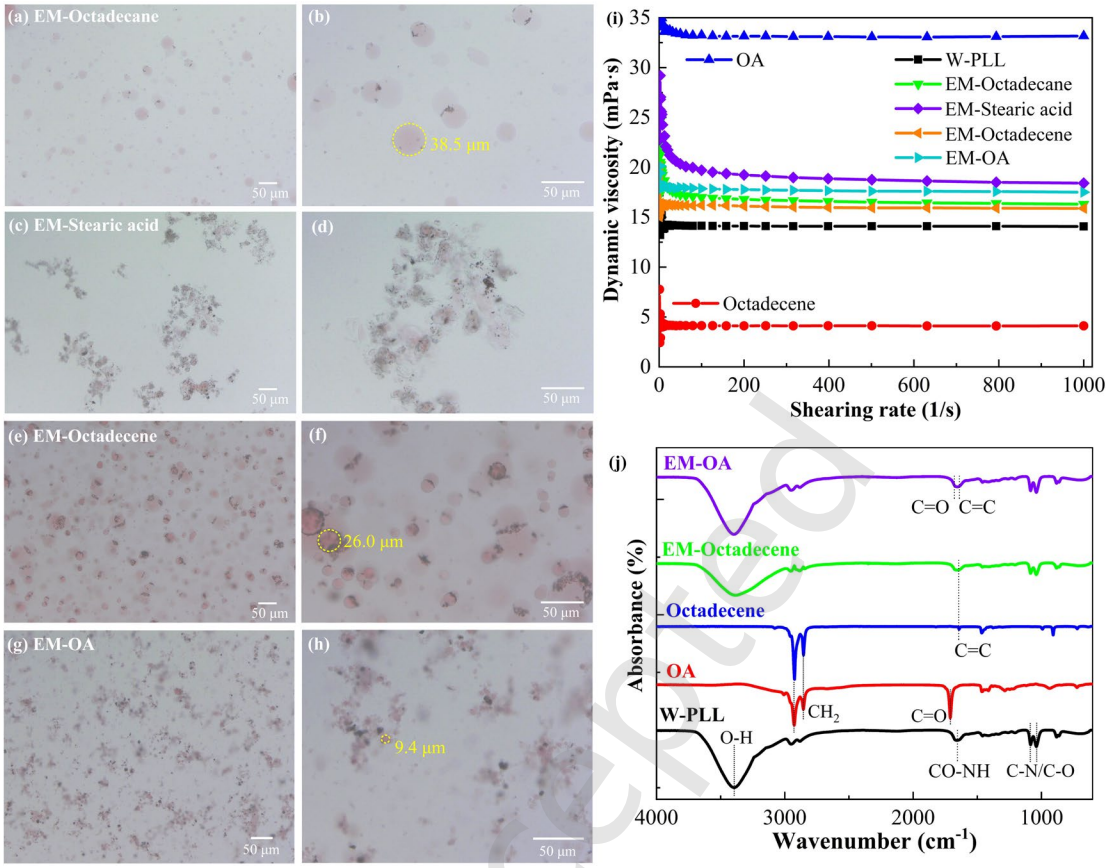

Fig. 1. Characterization of the prepared emulsions (1.0 wt% oil concentration). (a-b) Micrographs of EM-octadecane emulsion. (c-d) Micrographs of EM-stearic acid emulsion. (e-f) Micrographs of EM-Octadecene emulsion. (g-h) Micrographs of EM-OA emulsion. (i) Dynamic viscosity. (j) FTIR spectra.

3.2 Friction performance

The COF evolutions of the steel/steel friction pair with the lubrication of W-PLL, oil, and emulsions were measured (Fig. 2a), respectively. The COF was around 0.027 with the lubrication of W-PLL. With the lubrication of oil phase OA and octadecene, the COF was larger than that of aqueous phase, which was about 0.06 and 0.10, respectively. When the oil phase was mixed with the aqueous phase to obtain the emulsion, the stabilized COFs were lower than that of either the aqueous phase or the oil phase. With the lubrication of EM-OA, the COF was as low as 0.001 after a running-in period of about 300 s, and the superlubricity was successfully obtained. The stable COF was 0.007 with the lubrication of EM-octadecene, and although the superlubricity

was also achieved, its COF was much larger than that of EM-OA. When EM-octadecane and EM-stearic acid were used for lubrication, the COF was 0.014 and 0.02 respectively, and no superlubricity was achieved.

To investigate the conditions for the superlubricity, the concentration of oil was first studied, with the results showing that the superlubricity could be achieved with an oil concentration in the range of 0.5-2.0 wt% for EM-OA and EM-octadecene lubrications, and the superlubricity state would be damaged when the concentration was greater than 3.0 wt% (Fig. 2b). This was consistent with the oil droplet distribution in Fig. S1, where the size of the 3.0 wt% droplets became much larger and the oil phase occupied a larger proportion. For EM-octadecane lubrication, only a 0.5 wt% oil concentration could realize superlubricity, and superlubricity failed above this concentration. In the case of EM-stearic acid lubrication, superlubricity could not be achieved regardless of the oil concentration.

The applied load also had a considerable effect on the superlubricity. When the normal load for EM-OA lubrication was increased from 1 N to 4 N, the COF increased slightly, all of which remained around 0.001. The COF increased to 0.011 when the normal load was further increased to 5 N, implying the damage of the superlubricity state. The superlubricity could be maintained at 1-4 N with COFs ranging from 0.004 to 0.007 for EM-octadecene lubrication, while the COF reached 0.012 at 5 N, indicating superlubricity failure. The COF was around 0.01 at 1-3 N for EM-octadecane lubrication, and it reached 0.014 and 0.023 at 4 N and 5 N, respectively. For the EM-stearic acid lubrication, the COF was around 0.02 at 1-4 N, and it reached 0.031 at 5 N.

Finally, the superlubricity performance was also investigated under variable speeds during the friction tests (Fig. 2d). When the sliding speed was in the range of 0.025-0.065 m/s, a decrease in COF was observed as the sliding speed increased for all emulsions. When the sliding speed was greater than 0.065 m/s, the COF did not continue to increase. Only when the sliding speed was greater than 0.065 m/s, the

superlubricity with COFs of 0.001 and 0.007 could be realized for EM-OA and EM-octadecene lubrications, respectively.

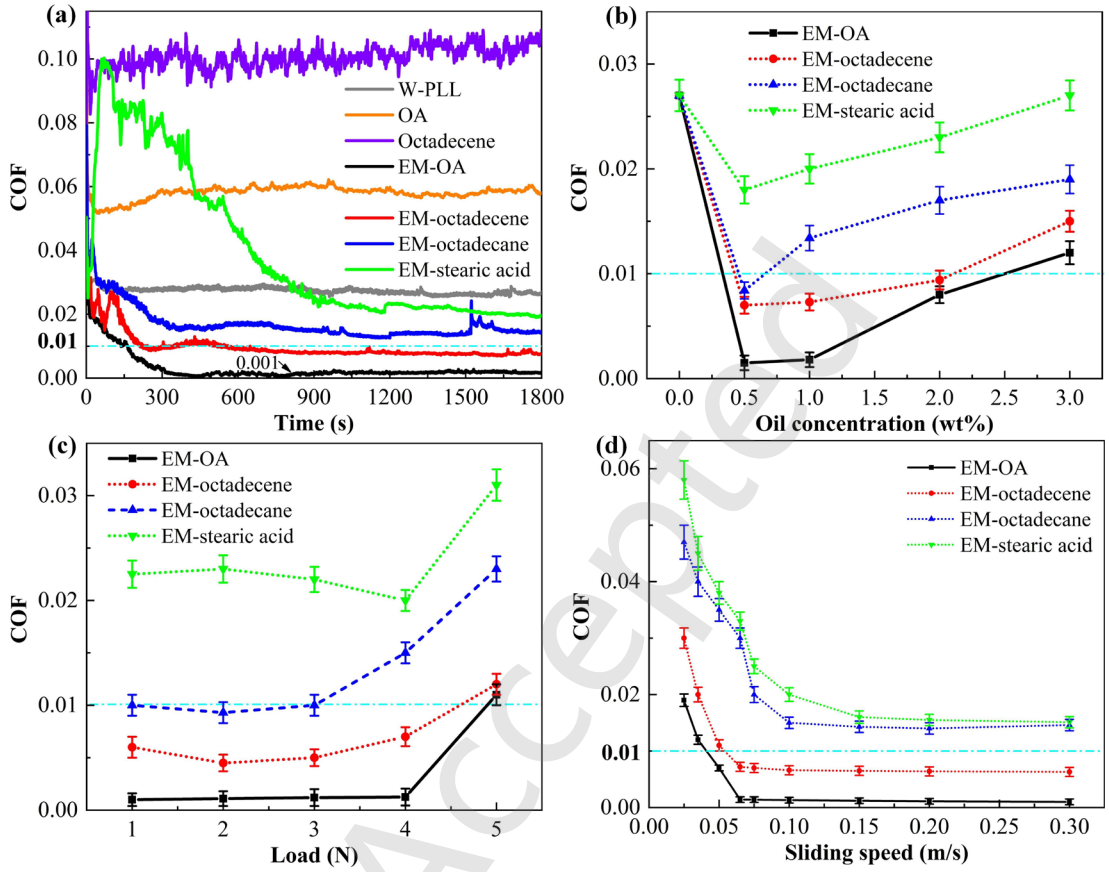

Fig. 2. (a) COFs with the lubrication of W-PLL, Oil and emulsions (4 N, 0.1 m/s, 1.0 wt% oil concentration). (b) Comparison of COFs at varying oil concentrations. (c) Comparison of COFs at different loads with the lubrication of different emulsions. (d) Comparison of COFs at different sliding speeds with the lubrication of different emulsions.

3.3 Wear properties

The wear scars of the ball and disk surfaces after the lubrication of W-PLL, OA, EM-octadecene, and EM-OA were measured by the 3D white light interferometer (Fig. 3), respectively. The wear scar diameters after the lubrication of W-PLL, OA, EM-octadecene, and EM-OA were 223, 132, 216, and 161 μm, respectively (Fig. 3a-d). With the lubrication of OA, the wear scar diameter was the smallest among all lubricants. When EM-OA was used for lubrication, the wear scar diameter was the smallest among the emulsions (Fig. 3a-d and Fig. S3a-c). The average contact pressure (ratio of load to

wear scar area) in the superlubricity state with the lubrication of EM-octadecene and EM-OA reached 109 and 197 MPa respectively. Meanwhile, the ball wear scar cross-section curves indicated that the ball wear depth with the lubrication of EM-OA was also the smallest among the emulsions, as shown in Fig. 3(i) and Fig.S3(g). For the surfaces lubricated by EM-octadecene (Fig. 3c) and EM-octadecane (Fig. S3b), the ball wear scar diameter of the EM-octadecene that achieved superlubricity was also smaller than that of the EM-octadecane that did not achieve superlubricity. Compared with EM-octadecane, EM-octadecene only had an additional carbon-carbon double bond in the molecular structure of the oil phase, so it could be inferred that the carbon-carbon double bond was conducive to reducing friction and wear.

For the steel disk surface, the depth and width of the wear scar were smaller after the lubrication of EM-OA, which demonstrated excellent wear resistance (Fig. 3e-h and Fig. S3d-f). It is noteworthy that the middle region of the wear scar on the disk surface after the lubrication of EM-OA was smoother. This region exhibited the lowest roughness (26.3 nm). On both sides of the wear scar, a black material different from the steel matrix appeared. The cross-section curves fluctuated more in this region, which could be the accumulation of fine wear chips. A similar black substance also appeared at the same location on the steel surface after the lubrication of EM-stearic acid (Fig. S3f), but its distribution was not as uniform as that of EM-OA. This phenomenon did not occur under any other lubrication conditions. The unique feature of EM-OA and EM-stearic acid was the presence of carboxyl groups in their oil phases, from which it could be inferred that the presence of carboxyl groups induced the formation of black substances.

Combined with the aforementioned comparison of ball wear scar diameters, the carbon-carbon double bond in the OA molecules was favorable for anti-wear performance. Therefore, the reason for EM-OA to achieve superlubricity was likely attributable to the synergistic effect of the carbon-carbon double bond and the carboxyl group in the OA molecule, the carboxyl group promoted the formation of a uniform

black protective layer on the wear surface, whereas the carbon-carbon double bond contributed additionally to the anti-wear performance.

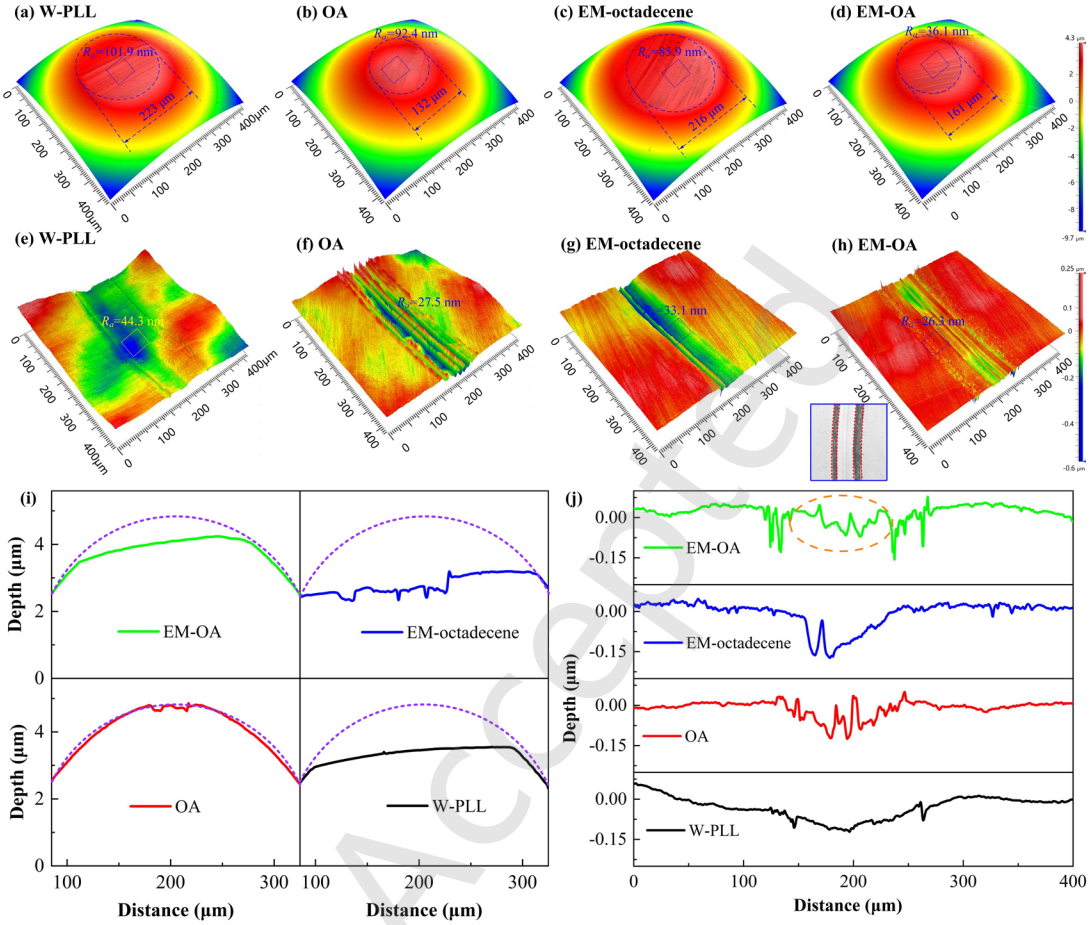

Fig. 3. Images of the worn surfaces lubricated by different liquids obtained by the 3D white-light interferometer. (a-d) Images on the steel ball surfaces. (e-h) Images on the steel disk surfaces. (i) Cross-sectional curves on the steel ball surfaces for different lubrications; (j) Cross-sectional curves on the steel disk surfaces for different lubrications.

3.4 Surface analyses

To illustrate the superlubricity mechanism, the XPS spectra of the wear scar regions on the steel disk surfaces were measured (Fig. 4). For the C 1s XPS spectra (Fig. 4a), there was a characteristic peak of peptide bonding (-CO-NH-) at 286. 0 eV on the steel surface after the lubrication of W-PLL, which belonged to the retention of PLL-derived moieties. The steel surface after the lubrication of OA showed a C=O peak at 288.5 eV, which corresponded to the carboxyl group in the OA molecules. The steel

surface after the lubrication of EM-OA also showed the peak of the C=O bond. There was a distinct characteristic peak at 283.5 eV, which corresponded to the C=C bond. Both C=O and C=C bonds belonged to the characteristic structure of OA molecules, which suggested that the OA molecules in the emulsion was adsorbed to the friction surface. For the N 1s XPS spectra (Fig. 4b), there was no response on the steel surface after the lubrication of OA. However, the presence of the amino group ($-NH_2$), a characteristic functional group of PLL molecules, was detected after the lubrication of W-PLL and EM-OA, indicating that PLL molecules in the emulsion were adsorbed onto the steel surface. The O 1s XPS spectra (Fig. 4c) reflected the oxidation that occurred on the steel surface and the adsorption of C=O bonds with the lubrication of EM-OA. Both Ce 3d and Cl 2p XPS spectra (Fig. 4d, e) after the lubrication of EM-OA showed signals, indicating the adsorption of emulsifier molecules on the steel surface. Notably, the Ce 3d spectrum (Fig. 4d) exhibited features characteristic of Ce^{4+} (CeO_2), rather than the Ce^{3+} state originally present in the DDCe emulsifier. This indicated a tribochemical oxidation reaction during friction ($Ce^{3+} \rightarrow Ce^{4+}$), forming CeO_2 on the steel surface, as evidenced by the characteristic satellite peak at 897.5 eV in the Ce 3d XPS spectrum. The formation of CeO_2 was crucial for superlubricity, as CeO_2 provided low shear strength and effectively reduced friction and wear. This interpretation aligned with Chen et al. [34], who also observed CeO_2 formation from a Ce^{3+} based microemulsion under friction. Meanwhile, the depth sputtering pattern of Ce 3d spectra (Fig. 4d) implied that the penetration depth of emulsifier molecules on the steel surface was about 40 nm.

In the wear track after the lubrication of EM-OA, there was a difference in the morphology between the edge and the center (the edge was enriched with fine particles, Fig. 4f). Therefore, EDS mapping of the wear track was performed and the results showed that the edges were enriched in the elements C, O, and Cl (Fig. 4g-k). The XPS spectra of the remaining three emulsions were shown in Fig. S4. They all exhibited similar N 1s and O 1s spectra, and the N 1s spectra indicated the presence of aqueous

phase molecules (-NH_2). It was worth noting that the surface after the lubrication of EM-octadecene that achieved superlubricity also exhibited C=C bonds (Fig. S4a, C 1s spectra) and emulsifier molecules (Fig. S4b, Cl 2p spectra). When the surface was lubricated with EM-octadecane and EM-stearic acid, no emulsifier molecules were present. At the same time, the lubricated surface of EM-stearic acid did not contain C=O bonds, indicating that the oil phase molecules were not adsorbed onto the friction interface. In contrast, the emulsifier molecules were not present on the surfaces lubricated with EM-octadecane and EM-stearic acid, which could not achieve superlubricity. Also, the C=O bond was not present on the surface after the lubrication of EM-stearic acid, indicating that the oil phase molecules were not adsorbed onto the friction interface. These results indicated that the surfaces after the lubrication of EM-OA and EM-octadecene that could achieve superlubricity adsorbed oil phase and emulsifier molecules, whereas those that could not achieve superlubricity showed no adsorption of emulsifier and corresponding oil phase molecules.

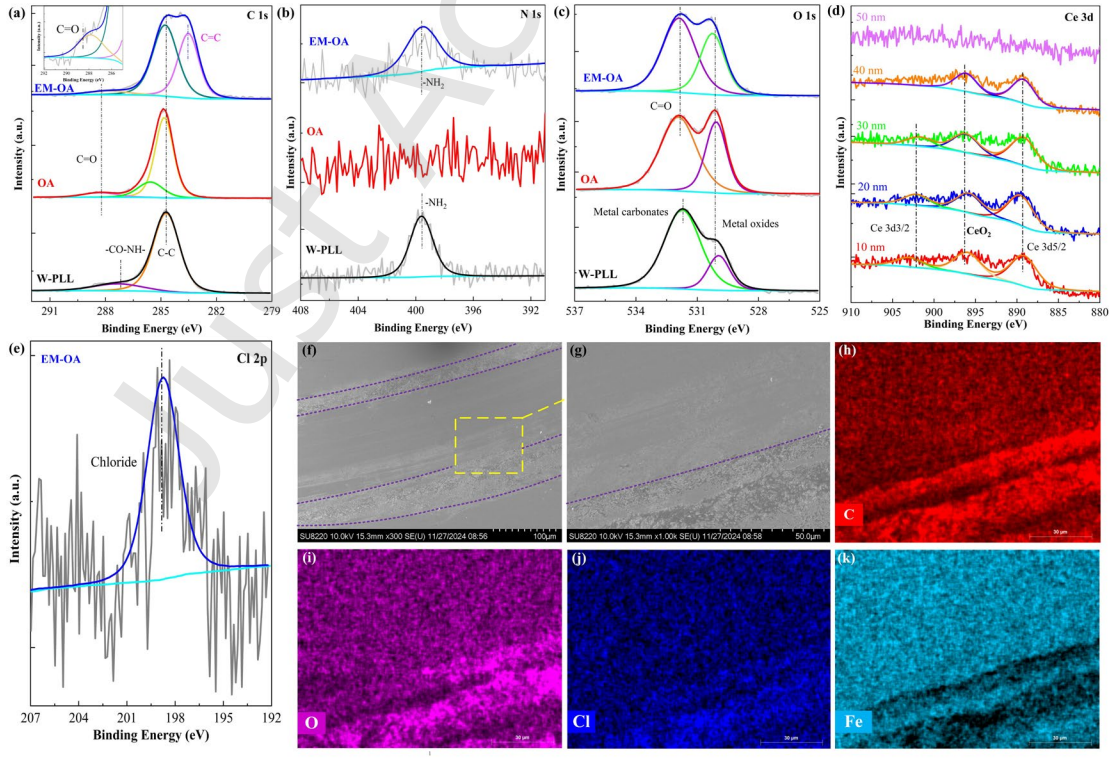

Fig. 4. XPS spectra on the steel disk surfaces. (a) C 1s spectra. (b) N 1s spectra. (c) O 1s spectra. (d) Ce 3d spectra. (e) Cl 2p spectra. (f, g) SEM images of the wear track on the steel disk surface lubricated by EM-OA. (h-k) EDS mapping of C, O, Cl and Fe elements on the steel disk surface.

In order to observe the molecular derivatives adsorbed on the friction surface and the tribofilm, the cross-section of the wear scar area on the steel disk surface lubricated with EM-OA was prepared by FIB and observed by HRTEM. As shown in Fig. 5, a tribofilm with a thickness of about 41.3 nm existed on the steel disk, and the magnified observation of the tribofilm region revealed regular lattice in HRTEM. The fast Fourier transform indicated the lattice spacings of the marked regions were 0.242 and 0.264 nm (Fig. 5b), which correspond to the (222) and (310) crystal planes of Fe_2O_3 (JPCDS#39-1346), respectively. The line and surface scan analysis of the tribofilm region showed that there were O, Fe, C, and Cl elements, with the Cl element originating from the added emulsifier. This suggested that the tribofilm was mainly composed of adsorbed emulsion molecules, Fe_2O_3, and friction chemical reaction products.

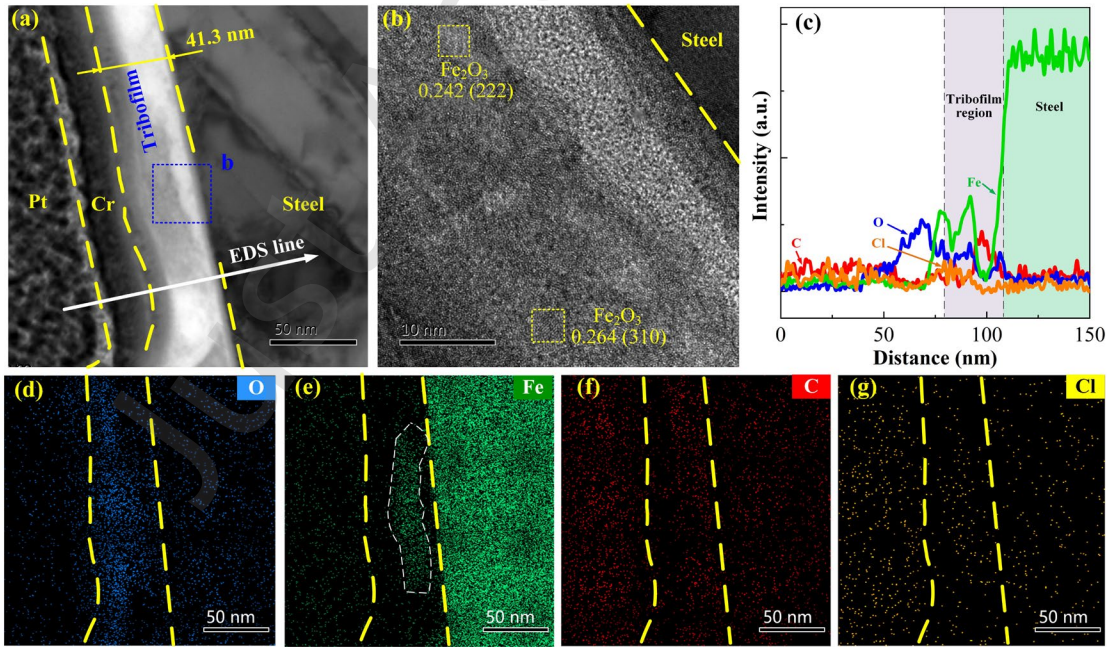

Fig. 5. TEM analysis of the cross-sections in the wear scar regions on the steel disk surface after the lubrication of EM-OA. (a) TEM images of the cross-section in the wear scar region. (b) HRTEM images of the cross-section in the wear scar region. (c) Elemental distribution of O, Fe, C and Cl along the EDS line. (d-g) EDS mapping of O, Fe, C and Cl elements in the wear scar region.

3.5 Superlubricity mechanisms

In emulsions with 18 carbon atom olefins as the oil phase, the carbon-carbon double bonds and carboxyl groups of the oil phase contributed to the realization of superlubricity. To further investigate the effect of emulsion composition on superlubricity, the emulsifier and aqueous phases in the EM-OA emulsion were replaced separately, and then additional supplementary experiments were conducted. Firstly, the emulsifiers were replaced with Span80 and sodium dodecyl benzene sulfonate (SDBS) to prepare the emulsions, and tribological tests were conducted under the same working conditions as EM-OA lubrication (4 N, 0.1 m/s, 0.1 wt%). The experimental results were shown in Fig. S5(a), where the emulsion with Span80 as an emulsifier failed to achieve superlubricity as the COF stabilized at about 0.03 after about 1200 s of running-in period. The emulsion prepared with SDBS emulsifier was stabilized at a COF of about 0.012 after about 300 s of running-in period. Although SDBS also failed to achieve superlubricity, there was a lower COF and a shorter running-in period. This suggested that the presence of the dodecyl group was favorable for COF reduction because both SDBS and DDCE possessed similar straight chain alkyl groups with 12 carbon atoms.

Secondly, the PLL in the aqueous phase of EM-OA was replaced with other types of amino acids such as polyaspartic acid, polyglutamic acid, and lysine. Similarly, tribological tests were performed under working conditions consistent with EM-OA. The experimental results were shown in Fig. S5(b), where polyaspartic acid and lysine exhibited a shorter running-in period and stabilized with a COF of about 0.08, while polyglutamic acid stabilized at a COF of around 0.04 after a running-in period of about 1200 s. The properties of these various aqueous phases were compared in Table S1. This indicated that PLL was not replaceable and only its use as an aqueous phase could realize superlubricity. It might be due to its rich amino functional groups, which enabled strong adsorption and tribochemical reactions with metal surfaces. In contrast, polyaspartic acid contained only carboxyl groups on the surface without amino groups.

The monomeric lysine contained both amino and carboxyl groups, but in smaller amounts. The polyglutamic acid contained both carboxyl and amino groups, but it was possible that the presence of the carboxyl group reduced the effect of the amino group.

The failure of these PLL-replacement experiments underscored the unique role of PLL in achieving superlubricity. PLL was a polymeric amino acid with abundant ε-amine ($–NH_2$) side chains along its backbone, enabling multi-point anchoring to the steel surface via strong Fe–N coordination or hydrogen bonding. This formed a dense and shear-resistant chemisorbed layer that served as the essential foundation for the subsequent growth of the composite tribofilm—a function that other amino acids could not fulfill due to their limited anchoring capability (as reflected by the significantly higher COFs in Fig. S5b).

The working condition with the lubrication of EM-OA was used to calculate the lubrication film thickness using the Hamrock-Dowson formula and determine the lubrication state of superlubricity [35, 36]. At a load of 4 N and a sliding speed of 0.1 m/s, the minimum lubrication film thickness was 10.5 nm (Supporting Information). Simultaneously, the ratio of the film thickness to the equivalent surface roughness of the friction pair was 0.24, confirming that the superlubricity state was realized in the boundary lubrication regime. In the boundary lubrication state, the lubrication film thickness was very thin, much less than the contact surface roughness, and the lubrication film was not sufficient to completely cover and separate the two contact surfaces. In this case, the lubrication performance mainly depended on the quality of the generated tribofilm, which was crucial for the realization of superlubricity. Therefore, the superlubricity mechanism was attributed to the tribofilm generated by the tribochemical reaction between the water phase, oil phase and emulsifier and the friction interface. As schematically illustrated in Fig. 6 (a), the EM-OA emulsion exhibited an oil-in-water (O/W) microstructure, with OA droplets (about 9.4 μm) uniformly dispersed in the continuous aqueous phase containing PLL and DDCe. Under friction, these droplets were disrupted, releasing OA, PLL, and DDCe molecules to the

steel surface, where they assembled into a hierarchical tribofilm (Fig. 6b). This tribofilm exhibited a hierarchical structure consisting of a thin chemisorbed foundation and a thicker composite tribofilm, as inferred from complementary XPS and HRTEM analyses. First, a robust chemisorbed layer formed directly on the steel surface, primarily through the strong interactions (e.g., Fe-O-C or Fe-N bonds) between the metal and the functional groups (–COOH of OA and $–NH_2$ of PLL). This chemisorbed layer served as a vital foundation, ensuring the firm adhesion and stability of the tribofilm. Upon this foundation, a thicker (about 40 nm) composite tribofilm grew incorporating nanocrystalline Fe_2O_3, cross-linked organic moieties from OA and PLL, and embedded species from the emulsifier (e.g., Ce, Cl). The presence of this hierarchical tribofilm hindered direct steel-to-steel contact, converting the friction interface into a tribofilm-to-tribofilm contact that provided low shear strength. In particular, the carbon-carbon double bonds and carboxyl groups in the oil phase had a large influence on the formation of the chemisorbed layer and the subsequent composite tribofilm and the realization of superlubricity. If they were lacking in the oil phase, superlubricity could not be realized, and the friction interface would not adsorb the oil phase molecules.

To better understand why OA achieved the best performance while other oil phases fail or perform poorly, the key properties of the four emulsions were compared in Table 1. All four emulsions showed similar viscosities (15.9-18.6 mPa·s), but their COFs varied dramatically (0.001–0.020), indicating that viscosity was not the determining factor. The chemical structure comparison revealed that the presence of both C=C and –COOH in OA was essential for achieving the lowest COF (0.001). Octadecene (C=C only) achieved a higher COF (0.007) but still reached superlubricity. In contrast, octadecane (no functional groups) and stearic acid (–COOH only) failed. These observations supported the proposed mechanism that the synergistic adsorption of C=C, –COOH, $–NH_2$ (PLL), and (DDCe) was essential for forming the hierarchical tribofilm that enabled macroscopic superlubricity.

Table 1 Comparison of the different emulsions

Emulsions	Dynamic viscosity (mPa·s)	Max droplet size (μm)	Min COF	Chemical structure
EM-OA	17.6	9.4	0.001	C=C and –COOH
EM-Octadecene	15.9	26.0	0.007	C=C only
EM-Octadecane	16.4	38.5	0.014	Neither
EM-Stearic acid	18.6	Irregular	0.020	–COOH only

The best oil phase concentration was 0.5-2.0 wt%, for which the oil droplets were uniformly distributed in the aqueous phase and remained small in size (maximum 9.4 μm at 1.0 wt%, Fig.S1), forming a uniform and stable emulsion. Under these conditions, the fine droplets served as efficient carriers, ensuring a continuous and homogeneous supply of OA and DDCe molecules to the friction interface. This steady delivery sustained the synergistic OA/PLL/DDCe adsorption balance required for the formation and replenishment of the hierarchical tribofilm, thereby maintaining stable superlubricity. At 2.0 wt%, the maximum droplet size increased to 14.1 μm, and the superlubricity state approached a critical threshold, as reflected by a larger COF (0.008, Fig. 2b). When the oil concentration was too high (3.0 wt%), the oil droplets grew significantly (maximum 22.5 μm, Fig.S1) and occupied a disproportionally large area fraction in the emulsion. Consequently, the delivery of functional components to the contact zone became intermittent and non-uniform. The arrival of a single large droplet could momentarily flood the narrow contact interface with an excess of OA, disrupting the optimal OA/PLL/DDCe ratio required for maintaining the structural integrity of the chemisorbed layer and the composite tribofilm. This disruption of the synergistic adsorption balance ultimately led to the failure of superlubricity. When the load was in the range of 1-4 N, the generated tribofilm exhibited good load-bearing capacity to realize superlubricity. When the load increased to 5 N, the tribofilm, especially its underlying chemisorbed layer, was not enough to withstand the greater pressure and

was destroyed, leading to the failure of superlubricity. In terms of sliding speed, when the rotational speed reduced to below 0.065m/s, the thickness of the liquid film was very thin, and the tribochemical activation was insufficient, so the tribochemical reaction was not violent enough to generate or sustain the tribofilm with good friction reduction performance. In this study, the EM-OA emulsion was used to realize the macroscopic superlubricity with a short running-in period, thereby providing excellent lubrication performance and inhibiting the wear of the friction pair, which provided a new path to develop the lubrication system with near-zero wear.

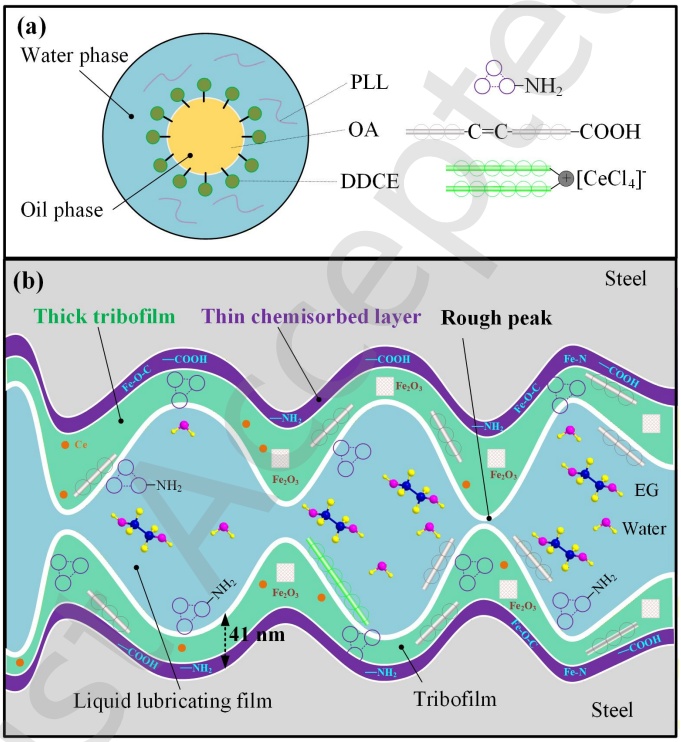

Fig. 6. Schematic diagram of the superlubricity mechanism with the lubrication EM-OA. (a) Emulsions and molecular structure. (b) The lubrication mechanism of EM-OA at the friction interface.

4 Conclusions

In summary, an emulsion was prepared using the PLL, OA, and a Ce-based emulsifier, which achieved macroscopic liquid superlubricity. The superlubricity state with a minimum COF of 0.001 and a maximum contact pressure of 197 MPa was

obtained after a running-in period of about 300 s. Systematic comparative experiments revealed that the superlubricity relied on the synergistic contribution of the oil phase (C=C/–COOH), the aqueous phase (–NH_2), and the Ce-based emulsifier, rather than any single component. Specifically, the C=C and –COOH groups in OA enhanced its chemisorption onto the steel surface and promoted the formation of a low-shear organic layer. PLL, through its abundant amino groups, provided strong interfacial binding and facilitated tribochemical reactions, thereby stabilizing the overall structure of the boundary film. DDCe not only stabilized the emulsion but also participated in interface formation. Its long dodecyl chains helped organize the adsorbed layer, while the Ce^{3+} ions might have reinforced the film's cohesion and load-carrying capacity. Together, these components enabled the growth of a hierarchical tribofilm consisting of a thin chemisorbed foundation and a thicker composite layer containing Fe_2O_3 nano crystallites and organic–inorganic hybrids, which effectively separated the sliding surfaces and provided ultralow shear resistance. This study has obtained very low friction and wear with the lubrication of an emulsion, which has great application potential in mechanical engineering lubrication.

Acknowledgment

The work was financially supported by the National Natural Science Foundation of China (No. 52488101, 52175174), the Beijing Natural Science Foundation (No. JQ25011), the Natural Science Foundation Project of Sichuan Province (No. 2025NSFSC2053), the Jiangsu Provincial Key Laboratory Project for Market Supervision (No. JSTJ-KFKT-QZ2025005), and the Talent Introduction Program of Xihua University (No. ZX20260030).

References

[1] Holmberg K, Erdemir A. Influence of tribology on global energy consumption, costs and emissions. *Friction*.**5** (3):263-284(2017)

[2] Chhowalla M, Amaratunga GA. Thin films of fullerene-like MoS2 nanoparticles with ultra-low friction and wear. *Nature*.**407** (6801):164-167(2000)

[3] Zhou Z. Tribology in China. *Friction*.**13** (1):9440994(2025)

[4] Saravanan P, Selyanchyn R, Tanaka H, Darekar D, Staykov A, Fujikawa S, et al. Macroscale Superlubricity of Multilayer Polyethylenimine/Graphene Oxide Coatings in Different Gas Environments. *ACS Appl Mater Interfaces*.**8** (40):27179-27187(2016)

[5] Han T, Zhang C, Luo J. Macroscale Superlubricity Enabled by Hydrated Alkali Metal Ions. *Langmuir*.**34** (38):11281-11291(2018)

[6] Tang H, Deng W, Li J, He J, Chen X. Critical advances in superlubricity: From current challenges to sustainable development beyond laboratory. *Friction*.**13** (10):9441075(2025)

[7] Jang S, Chen Z, Kim SH. Origin of superlubricity of diamond-like carbon (DLC). *Friction*.**13** (1):9440995(2025)

[8] Zubieta-Laborde PM, Long Y, Lubrecht T, Cross GLW, Dubreuil F, Martin JM, et al. Hypericin enhances superlubricity of glycerol by acting as graphene precursor. *Friction*.**13** (1):9441018(2025)

[9] Li J, Zhang C, Luo J. Superlubricity behavior with phosphoric acid-water network induced by rubbing. *Langmuir*.**27** (15):9413-9417(2011)

[10] Li J, Zhang C, Ma L, Liu Y, Luo J. Superlubricity achieved with mixtures of acids and glycerol. *Langmuir*.**29** (1):271-275(2013)

[11] Ma Q, He T, Khan AM, Wang Q, Chung YW. Achieving macroscale liquid superlubricity using glycerol aqueous solutions. *Tribol Int*.**160**:107006(2021)

[12] Chen Z, Liu Y, Zhang S, Luo J. Controllable superlubricity of glycerol solution via environment humidity. *Langmuir*.**29** (38):11924-11930(2013)

[13] Ma Q, Liang M, Xu X, Yan C, Wang H. Towards direct superlubricity and negligible wear with polyalcohol lubricant mixtures of ethylene glycol and glycerol for steel tribopairs. *Appl Surf Sci*.**663**:160151(2024)

[14] Wang HD, Liu YH, Li JJ, Luo JB. Investigation of Superlubricity Achieved by Polyalkylene Glycol Aqueous Solutions. *Adv Mater Interfaces*.**3** (19):1600531(2016)

[15] Hua J, Björling M, Larsson R, Shi YJ. Controllable superlubricity achieved with mixtures of green ionic liquid and glycerol aqueous solution via humidity. *J Mol Liq*.**345**:117860(2022)

[16] Zheng ZW, Liu XL, Yu HX, Chen HJ, Feng DP, Qiao D. Insight into macroscale superlubricity of polyol aqueous solution induced by protic ionic liquid. *Friction*.**10** (12):2000-2017(2022)

[17] Zheng QK, Chhattal M, Bai CN, Zheng ZW, Qiao D, Gong ZB, et al. Superlubricity of PTFE triggered by green ionic liquids. *Appl Surf Sci*.**614**:156241(2023)

[18] Liu Y, Li J, Ge X, Yi S, Wang H, Liu Y, et al. Macroscale Superlubricity Achieved on the Hydrophobic Graphene Coating with Glycerol. *ACS Appl Mater Interfaces*.**12** (16):18859-18869(2020)

[19] Ge X, Li J, Luo R, Zhang C, Luo J. Macroscale Superlubricity Enabled by the Synergy Effect of Graphene-Oxide Nanoflakes and Ethanediol. *ACS Appl Mater Interfaces*.**10** (47):40863-40870(2018)

[20] Zeng QF, Yu F, Dong GN. Superlubricity behaviors of Si3N4/DLC Films under PAO oil with nano boron nitride additive lubrication. *Surf Interface Anal*.**45** (8):1283-1290(2013)

[21] Wang W, Xie GX, Lueir JB. Superlubricity of Black Phosphorus as Lubricant Additive. *Acs Appl Mater Inter*.**10** (49):43203-43210(2018)

[22] Du S, Zhang C, Luo Z. Study on the effect of diketone lubricant on the tribological properties of angular contact ball bearing with skidding behavior. *Friction*.9441214(2026)

[23] Ma Q, Yan C, Xu X, Liang M, Hua K, Wang H. Insight into remarkable oil superlubricity enabled by polyether-modified silicone oil on engineering steel. *Friction*.**13** (9):9441034(2025)

[24] Wei P, Hou X, Han S, Wen X, Zhou X, Meng Y, et al. Superlubrication of poly-α-olefin-8 (PAO8) enabled by MXene/PI coating. *Friction*.**13** (6):9440967(2025)

[25] Eskandari M, Macknojia AZ, Shirani A, Chapman K, Berman D. Toward lithium-free tribology: Design and performance of plant oil-based greases thickened with functionalized nanoclays. *Friction*.9441204(2025)

[26] Duan C, Li D, Gu J, Gao C, Zhang S, Zhang P, et al. Smart polymer self-lubricating material: Optimal structure of porous polyimide with base oils for super-low friction and wear. *Friction*.**13** (8) (2025)

[27] Du S, Zhang C, Luo Z. Combination of diketone and PAO to achieve macroscale oil-based superlubricity at relative high contact pressures. *Friction*.**12** (5):869-883(2024)

[28] Wang J, Gao C, Duan C, Yang G, Ma J, Yu L, et al. Whole course oil-based superlubricity for polyetheretherketone-bearing steel sliding pair by introducing tribocatalytically active dialkyl-dithiophosphoric-modified copper nanoparticles in poly-alpha olefin oil. *Friction*.**13** (5):9440954(2025)

[29] Li JY, Yuan YY, Amann T, Yuan CQ, Li K. Macroscopic Oil-Based Superlubricity Achieved on Steel Surfaces with the Roughness of Engineering Level. *Tribology Letters*.**71** (2):1-10(2023)

[30] Zeng Q, Dong G, Martin JM. Green superlubricity of Nitinol 60 alloy against steel in presence of castor oil. *Sci Rep*.**6**:29992(2016)

[31] Long Y, Wang Y, Weihnacht V, Makowski S, Kubo M, Martin JM, et al. Mechanism of superlubricity of a DLC/Si3N4 contact in the presence of castor oil and other green lubricants. *Friction*.**10** (10):1693-1706(2022)

[32] Gao K, Jiao JG, Wang Z, Xie GX, Luo JB. Superlubricity induced by partially oxidized black phosphorus on engineering steel. *Friction*.**11** (9):1592-1605(2023)

[33] Yi S, Li JJ, Rao JS, Ma XY, Zhang YX. Alkyl-functionalized black phosphorus nanosheets triggers macroscale superlubricity on diamond-like carbon film. *Chem Eng J*.**449**:137764(2022)

[34] Chen S, Sun H, Liu J, Wang J, Lu H, Hao J, et al. A dual-responsive microemulsion with macroscale superlubricity and largely switchable friction. *Mater Horiz*.**11** (7):1668-1678(2024)

[35] Ge XY, Li JJ, Wang HD, Zhang CH, Liu YH, Luo JB. Macroscale superlubricity under extreme pressure enabled by the combination of graphene-oxide nanosheets with ionic liquid. *Carbon*.**151**:76-83(2019)

[36] Liu Y, Yu S, Li J, Ge X, Zhao Z, Wang W. Quantum dots of graphene oxide as nano-additives trigger macroscale superlubricity with an extremely short running-in period. *Materials Today Nano*.**18**:100219(2022)